

DeNetDM: Debiasing by Network Depth Modulation

Silpa Vadakkeveetil Sreelatha*, Adarsh Kappiyath*, Anjan Dutta

University of Surrey, UK

Abstract. When neural networks are trained on biased datasets, they tend to inadvertently learn spurious correlations, leading to challenges in achieving strong generalization and robustness. Current approaches to address such biases typically involve utilizing bias annotations, reweighting based on pseudo-bias labels, or enhancing diversity within bias-conflicting data points through augmentation techniques. We introduce DeNetDM, a novel debiasing method based on the observation that shallow neural networks prioritize learning core attributes, while deeper ones emphasize biases when tasked with acquiring distinct information. Using a training paradigm derived from Product of Experts, we create both biased and debiased branches with deep and shallow architectures and then distill knowledge to produce the target debiased model. Extensive experiments and analyses demonstrate that our approach outperforms current debiasing techniques, achieving a notable improvement of around 5% in three datasets, encompassing both synthetic and real-world data. Remarkably, DeNetDM accomplishes this without requiring annotations pertaining to bias labels or bias types, while still delivering performance on par with supervised counterparts. Furthermore, our approach effectively harnesses the diversity of bias-conflicting points within the data, surpassing previous methods and obviating the need for explicit augmentation-based methods to enhance the diversity of such bias-conflicting points. Source code will be available upon acceptance.

1 Introduction

Deep neural networks (DNNs) have made remarkable progress over the past years in many different fields by delivering superior performance on large-scale datasets. However, while the benefits of training DNNs on large-scale datasets are undeniable, these algorithms also tend to inadvertently acquire unwanted biases [28]. Such biases can lead to systematic and unfair predictions based on certain attributes or groups, often reflecting societal prejudices. For instance, a classifier predominantly trained to recognize camels in desert landscapes could encounter difficulties when attempting to identify a camel situated on a road [15]. However, it is worth noting that not all biases are necessarily unwanted; some level of bias can be beneficial for model performance, such as the grounded assumption that cars typically operate on roads [4]. Nevertheless, identifying the unwanted biases and mitigating them is of utmost importance.

⁰ ** indicates authors with equal contribution

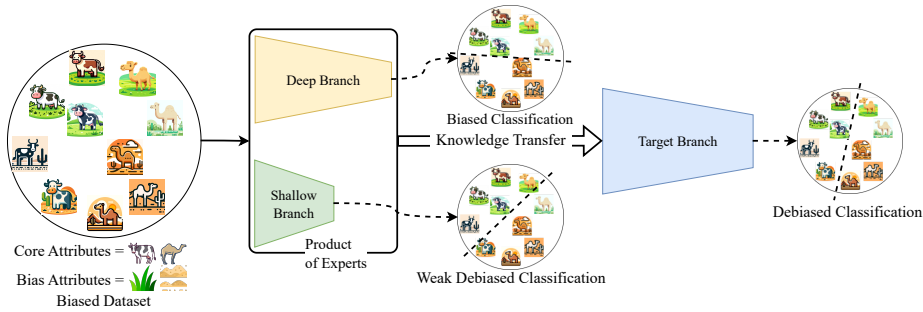


Fig. 1: Our DeNetDM model comprises a Product of Expert (PoE) [11], featuring one deep and one shallow expert. The shallow expert primarily captures core attributes, achieving debiased classification, while the deep expert focuses on bias. To compensate for the shallow expert’s limited capability due to less depth, we implement a knowledge transfer strategy utilizing knowledge from the experts to train a target debiased model.

Image classifiers, in particular, are prone to capture spurious correlations within the available data, hampering their generalization and robustness. Previous efforts to address this issue have typically depended on having prior knowledge of the bias. Certain methods assume the availability of bias annotations as suggested in [14, 21, 26, 34], and may involve predefined bias types, such as texture bias mitigation approach in [8], which limits models’ ability to address biases without prior knowledge. However, acquiring bias labels with human resources is expensive, time-consuming, and laborious. Recent studies, including [23] and [16], have shifted towards debiasing methods without bias labels, with approaches like [23] emphasizing bias-aligned samples and reweighting bias-conflicting samples, while others like [15, 16] introduce augmentation strategies to diversify bias-conflicting data points.

We aim to propose a novel approach that automatically identifies and mitigates spurious correlations of image classifiers without relying on explicit data augmentation or reweighting. To achieve this objective, we propose the DeNetDM (**D**ebiasing by **N**etwork **D**ePTH **M**odulation) model, which is grounded on insights gained from our preliminary study on feature decodability, which quantifies the extent to which specific data attributes can be accurately and reliably extracted from a given dataset or signal. In our study, we focus on the feature decodability of bias and core attributes in the neural networks of varying depths, following the approach outlined in [10]. This involves training specific linear decoders dedicated to mapping penultimate features of neural networks to bias and core attribute labels respectively, utilizing unbiased datasets. Our observations in untrained neural networks reveal that the attribute decodability tends to diminish as the neural networks become deeper. Additionally, we investigate the variation in attribute decodability when employing Empirical Risk Minimization (ERM) based training on networks of different depths. This aspect of our study is particularly enlightening, as it sheds light on how training methodologies and network architectures jointly influence the ability of a model to discern between different types of data attributes. A detailed discussion of the experimental setting and the conclusions can be found in Sec. 3.1.

We hypothesize that when we design a task that requires a pair of deep and shallow branches to acquire separate information, the deep branch consistently prefers bias attributes while the shallow branch favors core attributes. In practice, we employ a technique derived from the Product of Experts [11], where one expert is deeper compared to the other as illustrated in Fig. 1. Empirical evidence and analysis demonstrate that the deep branch becomes perfectly biased and the shallow branch becomes relatively debiased by focusing solely on the core attributes by the end of the training. Since the shallow branch may lack the capacity to capture the nuances of the core attributes adequately due to less depth, we propose a strategy where we train a deep debiased model utilizing the information acquired from both deep (perfectly biased) and shallow (weak debiased) network in the previous phase. Our training paradigm efficiently facilitates the learning of core attributes from bias-conflicting data points to the debiased model of any desired architecture without the need for explicit reweighting or augmentation as done in the previous approaches.

In summary, we make the following contributions:

- We conduct a comprehensive analysis of the decodability of bias and core attributes across neural networks of different depths;
- Leveraging insights gained from the aforementioned experiments and observations, we introduce a novel debiasing method that involves training a pair of deep and shallow networks to obtain a desired debiased model.
- We perform extensive experiments and ablation studies on a diverse set of datasets, including synthetic datasets like Colored MNIST and Corrupted CIFAR-10, as well as real-world datasets, Biased FFHQ and BAR.
- Our results demonstrate the superiority of our approach over existing state-of-the-art methods, achieving an improvement in performance of approximately 5%.

2 Related Works

Several works, such as [8, 10, 22], have highlighted neural networks’ vulnerability to spurious correlations during empirical risk minimization training, and recent years have seen the emergence of various debiasing techniques, which can be categorized as follows.

Supervision on bias: A wide variety of approaches, such as [14, 21, 26, 34], operate under the assumption that bias labels are readily accessible for mitigating the required bias. Some specific approaches in this domain assume prior knowledge of the bias type instead of explicitly using the bias annotations. For instance, approaches, such as [7, 8, 33] delve into methods focused on mitigating texture bias. Recent works by [5, 12] apply the Product of Experts method to mitigate bias in natural language processing where they presume the availability of a biased expert. Nevertheless, this assumption has its limitations as obtaining bias labels can be a non-trivial and resource-intensive task, making it a less practical approach. In contrast, our proposed DeNetDM does not necessitate pre-access to bias labels or bias types; rather, it leverages diverse network architecture depths within the Product of Experts framework to implicitly capture information related to bias and core attributes.

Utilization of pseudo bias-labels: Instead of relying on explicit bias annotations, recent approaches obtain pseudo-labels through heuristics to identify biased samples. One notable heuristic suggests that biases that are easy to learn are captured in the early stages of training, and this approach has been adopted by several studies, including [16, 20, 23], and numerous others [15, 17, 31]. Nam *et al.* [23] employ generalized cross-entropy loss to identify and subsequently reweight bias-conflicting points. On the other hand, Lee *et al.* [16] augment the features of bias-conflicting points to achieve a debiased model, whereas Liu *et al.* [20] introduce logit correction and group mixup techniques to enhance the diversity of bias-conflicting samples. Another category of approaches which includes [30] and [27] acquire pseudo-bias labels through clustering in the feature space of biased networks. Our approach does not explicitly need to acquire pseudo-bias labels in advance, as they are implicitly employed by the training of DeNetDM to facilitate the learning of both biased and debiased models.

Dependence on network architectures: Diffenderfer *et al.* [6] employ lottery-ticket-style pruning algorithms for obtaining compressed robust architectures. Similarly, other approaches, such as [24, 35], introduce pruning algorithms to extract robust subnetworks. Meanwhile, Shrestha *et al.* [29] applies Occam’s razor principle to optimize network depth and visual regions, enhancing overall robustness. Our method falls within this category but differs in that we do not specifically target the discovery of robust subnetworks. Instead, we leverage the training dynamics of architectures with varying depths to enhance debiasing.

Ensemble Knowledge Distillation: Our work shares conceptual similarities with the domain of ensemble knowledge distillation, as explored by Asif *et al.* [3] and Allen-Zhu *et al.* [2]. They focus on distilling knowledge from an ensemble of teacher models with different parameter sizes to enhance the performance of a student model. Similarly, our approach involves utilizing models with varying depths to achieve an unbiased model. Different from the existing works, we solely distill knowledge from the shallow model, while transferring knowledge orthogonal to the biased deep model via the Product-of-Experts training paradigm.

3 DeNetDM

In response to the observations to be discussed in Sec. 3.1 regarding linear decodability, we introduce DeNetDM, a debiasing approach centered on network depth modulation. Our training process comprises two stages: initially, a deep and shallow network pair is trained using a training paradigm that originates from Products of Experts [11], yielding both biased and debiased models, which is detailed in Sec. 3.2. Subsequently, recognizing the limitations of the shallow debiased model in capturing core feature complexities due to its depth, we proceed to train a target debiased model, ensuring it possesses the same or higher depth compared to the deep biased model. This phase leverages information acquired from the biased and debiased models in the previous step, as elaborated in Sec. 3.3. An illustration of the proposed approach is provided in Fig. 3.

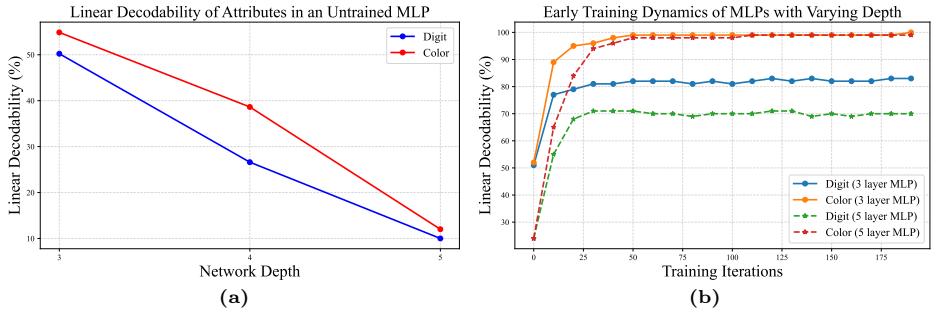


Fig. 2: Exploring the Effect of depth modulation: (a) illustrates how the linear decodability of features decreases as neural network depth increases, while (b) dives into the training dynamics of MLPs with varying depths under ERM.

3.1 Effect of Depth Modulation

This section presents an experimental investigation to gain insights into the impact of depth modulation of neural networks in the context of debiasing. We use the Colored MNIST dataset [23] (CMNIST), where digit identity (core attribute) is spuriously correlated with color (bias attribute).

We employ the concept of feature decodability to assess the extent to which the specific features of a given dataset can be reliably decoded from the models with varying depths. Hermann *et al.* [10] demonstrated that the visual features can be decoded from the higher layers of untrained models. Additionally, they observed that the feature decodability from an untrained model has a significant impact in determining which features are emphasized and suppressed during the model training. Following their approach, we specifically focus on assessing the decodability of bias and core attributes from the penultimate layer of untrained models. In order to evaluate the decodability of an attribute in a dataset, we train a decoder to map the activations from the penultimate layer of a frozen, untrained model to attribute labels. The decoder comprises a single linear layer followed by a softmax activation function. The decoder is trained using an unbiased validation set associated with the dataset, where each instance is labeled according to the attribute under consideration. Subsequently, the linear decodability of the attribute, measured in accuracy, is reported on the unbiased test set. We investigate the decodability of digit and color attributes in the CMNIST dataset from MLP models with varying depths, including 3, 4, and 5 layers, and the results are depicted in Fig. 2a. An intriguing observation is that the decodability of both attributes decreases as the depth of the neural network increases, which is also observed in [10]. To investigate how feature decodability evolves during the early stages of Empirical Risk Minimization (ERM) training across networks with varying depths, we train 3-layer and 5-layer MLPs on the CMNIST dataset. Following the training, we evaluate the model’s linear decodability for digit and color attributes. The results are summarized in Fig. 2b.

As observed in Fig. 2b, the initial phases of training for both networks emphasize color attribute (since bias is easy to learn), resulting in a notable enhancement in the decodability of color in both models. Also, as the training

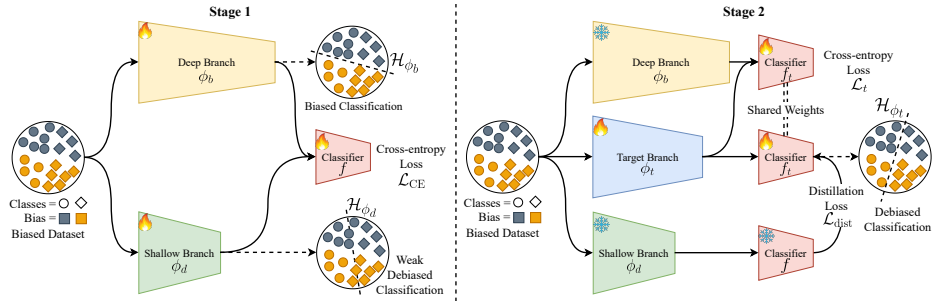


Fig. 3: Illustration of the DeNetDM framework: In Stage 1, an ensemble of shallow and deep branches produces outputs linearly combined and trained as a product of experts. The cross-entropy loss with depth modulation aids in separating biases and identifying target attributes. In Stage 2, we further introduce a target branch with the desired architecture, which also requires debiasing. This phase exclusively focuses on refining the target branch’s feature extractor (ϕ_t) and classifier head (f_t) while leveraging knowledge from the initial stages.

progresses, the decodability of the digit is higher in a 3-layer model when compared to a 5-layer model. Hence, the disparity in decodability between color and digit attributes becomes significantly more pronounced in a 5-layer MLP in comparison to a 3-layer MLP. Drawing upon these observations, our intuition is as follows: the significant gap in the linear decodability of bias and core attributes in the deep models might incline them towards favoring bias attributes while providing shallow models the opportunity to focus on core attributes when forced to capture distinct information.

This prompts us to explore whether similar behavior can be induced in models of equal depth. In this scenario, both models, undergoing ERM training, may exhibit a similar trend, with the disparity in decodability between biased and core attributes becoming nearly identical in both models due to same depth. Consequently, when we compel each model to learn distinct information, either model may capture biased or core attributes, or they might even divide the attribute information between them. This leads to a loss of control over the bias identification process. We also present empirical evidence in Sec. 4.4 to support these claims. Therefore, using models of different depths introduces an inductive bias suitable for the bias identification process, where deep and shallow models tend to capture biased and core attributes, respectively. Based on this rationale, we introduce the DeNetDM framework.

3.2 Stage1: Segregation of Bias & Core Attributes

In this section, we explain the training procedure to obtain the biased and debiased classifier for an M class classification problem. Let ϕ_b and ϕ_d denote the parameters of the feature extractors associated with the deep and shallow branches, where $\text{depth}(\phi_b) > \text{depth}(\phi_d)$. We use f to represent the classifier head shared by ϕ_b and ϕ_d . Here, f , ϕ_b and ϕ_d are trainable parameters. Considering an image-label pair (x, y) , the objective function is expressed as:

$$\mathcal{L}_{\text{CE}}(\hat{p}, y) = - \sum_{c=1}^M y_c \log(\hat{p}_c) \quad (1)$$

$$\hat{p} = \text{softmax}(f(\alpha_b \phi_b(x) + \alpha_d \phi_d(x)))$$

$$\text{If } \alpha_b = \alpha_d = 1, \quad \hat{p} = \text{softmax}(f(\phi_b(x) + \phi_d(x))) \quad (2)$$

where α_b and α_d are set to 1 throughout the training process. To evaluate the performance of an individual expert, we assign a value of 1 to the corresponding α while setting the other α equal to 0.

Our training methodology is derived from the Products of Experts technique [11] where multiple experts are combined to make a final prediction, and each expert contributes to the prediction with a weight. However, in our approach, the role of the experts is assumed by ϕ_b and ϕ_d , whose features are combined through weighted contributions. The conjunction of features is then passed to the shared classifier to generate predictions. We provide a detailed proof elucidating the derivation of Eq. (2) through the Product of Experts in Section B of the supplementary material. Due to the architectural constraints we imposed by modulating their capacities, the deep expert tends to prioritize the learning of bias attribute, while the shallow expert is inclined towards the core attribute. The model leverages the strengths of both experts to effectively learn from their combined knowledge. We investigate the training dynamics in Sec. 4.3.

3.3 Stage2 : Training the Target Debaised Model

The initial phase effectively separates the bias and core attributes into deep and shallow branches, respectively. However, relying solely on the debaised shallow branch may not be practical, as it might not capture the complex features representing the core attributes, given the less depth of the shallow model. This limitation does not apply to the deep biased model. To tackle this challenge, we introduce a target branch with the desired architecture for debiasing.

Let ϕ_t be the parameters of the feature extractor associated with the target branch and f_t be the classifier head whose weights are initialized using the weights of f . During this phase, our training is exclusively focused on ϕ_t and f_t . We freeze ϕ_b and ϕ_d since we leverage these models to only extract the necessary knowledge for debiasing the target branch. To capture information orthogonal to ϕ_b , we employ the same training approach described in Sec. 3.2, where ϕ_b and ϕ_t serve as the experts. The objective function can be written as:

$$\mathcal{L}_t(\hat{p}, y) = - \sum_{c=1}^M y_c \log(\hat{p}_c)$$

where,

$$\hat{p} = \text{softmax}(f_t(\beta_b \phi_b(x) + \beta_t \phi_t(x))) \quad (3)$$

The training and evaluation of the experts follow the procedure described in Sec. 3.2, with the key difference being that in this phase, only a single expert, ϕ_t , which is the target branch and classifier f_t , undergoes updates.

We further leverage the knowledge pertaining to the core attributes, which is encapsulated in ϕ_d , by transferring this knowledge to the target branch ϕ_t

through knowledge distillation. Here, ϕ_t acts as the student, whereas ϕ_d corresponds to the teacher. We set $\beta_b = 0$ and $\beta_t = 1$ in Eq. (3) to obtain the predictions of the student ϕ_t . Therefore, the distillation loss is given by :

$$\mathcal{L}_{\text{dist}}(\hat{p}_t, \hat{p}_s) = - \sum_{c=1}^M \hat{p}_{t_c} \log(\hat{p}_{s_c})$$

where, $\hat{p}_s = \text{softmax}\left(\frac{f_t(\phi_t(x))}{\tau}\right)$ (4) $\hat{p}_t = \text{softmax}\left(\frac{f(\phi_d(x))}{\tau}\right)$ (5)

Here, τ is the temperature which is a hyperparameter. Consequently, the complete loss function is given by :

$$\mathcal{L} = \mathcal{L}_t + \lambda \mathcal{L}_{\text{dist}} \quad (6)$$

where λ is a hyperparameter chosen from the interval $[0, 1]$. The pseudocode for the entire training process of DeNetDM is provided in Algorithm 1.

Algorithm 1 DeNetDM: Training

Input: Data: $\{(x, y)_i\}_{i=1}^N$
Output: ϕ_t, f_t
Initialize: $\phi_t, f_t, f, \phi_b, \phi_d$ such that $\text{depth}(\phi_b) > \text{depth}(\phi_d)$

- 1: **repeat**
- 2: Fetch minibatch data $\{(x, y)_i\}_{i=1}^K$
- 3: **for** $i = 1$ to K (in parallel) **do**
- 4: Compute \hat{p} using (2) to obtain $(\hat{p}, y)_i$
- 5: **end for**
- 6: Update ϕ_b, ϕ_d, f by minimizing \mathcal{L}_{CE} in (1) via SGD
- 7: **until** Convergence ▷ stage1
- 8: **repeat**
- 9: Fetch minibatch data $\{(x, y)_i\}_{i=1}^K$
- 10: **for** $i = 1$ to K (in parallel) **do**
- 11: Compute $\hat{p}, \hat{p}_s, \hat{p}_t$ via (3), (4), (5) respectively
- 12: **end for**
- 13: Update ϕ_t, f_t by minimizing \mathcal{L} in (6) via SGD
- 14: **until** Convergence ▷ stage2

4 Experiments

In this section, we discuss the experimental results and analysis to demonstrate the effectiveness of DeNetDM training in debiasing. We evaluate the performance of the proposed approach by comparing it with the previous methods in debiasing, utilizing well-known datasets with diverse bias ratios, consistent with the prior works in debiasing [16, 19, 23]. Additionally, we conduct an empirical study to analyze the training dynamics of DeNetDM. We also perform ablation studies to assess the impact and effectiveness of individual components within the proposed approach.

4.1 Experimental Setup

Datasets: We evaluate the performance of DeNetDM across diverse domains using two synthetic datasets (Colored MNIST [1], Corrupted CIFAR10 [9]) and two real-world datasets (Biased FFHQ [15], BAR [23]). In Colored MNIST (CMNIST), the digit identity is spuriously correlated with color, whereas in Corrupted CIFAR10 (C-CIFAR10), the texture noise corrupts the target attribute. Biased FFHQ (BFFHQ) consists of human face images and is constructed from the FFHQ dataset [13] such that the age attribute is spuriously correlated with gender. BAR consists of human action images where six human action classes are correlated with six place attributes. We conduct experiments with varying proportions of bias-conflicting points in the training set to demonstrate the efficacy of our approach across diverse scenarios. Following the experimental settings used by the previous works [16, 20, 25], we vary the ratio of bias-conflicting samples, specifically setting it at {0.5%, 1%, 2%, 5%} in the case of CMNIST and C-CIFAR10, {0.5%} in BFFHQ and {1%, 5%} in BAR datasets.

Baselines: We compare the performance of our proposed approach to the following bias mitigation techniques:

- **Empirical Risk Minimization (ERM)** [32]: Standard ERM using cross-entropy loss.
- **Group DRO (GDRO)** [26]: A supervised approach utilizing group labels to identify the worst group and learn an unbiased classifier.
- **Learning from Failure (LfF)** [23]: Identifies bias-conflicting points through the Generalized Cross Entropy (GCE) loss and upweighting for debiasing.
- **Just Train Twice (JTT)** [19]: Treating misclassified points by ERM-based classifiers as bias-conflicting and upweighting them for debiasing.
- **Disentangled Feature Augmentation (DFA)** [16]: Introducing feature augmentation to improve the diversity of bias-conflicting points and enhance unbiased accuracy.
- **Logit Correction (LC)** [20]: Proposes logit correction for bias mitigation along with MixUp [36] inspired data augmentation for increasing diversity.

Evaluation protocol: Evaluation of CMNIST and C-CIFAR10 is conducted on unbiased test sets, with target features being randomly correlated to spurious features. This evaluation protocol is commonly followed in the prior debiasing works [16, 19, 23]. Nevertheless, in the case of BFFHQ, we do not use the unbiased test set since half of them are bias-aligned points. In order to ensure a fair evaluation on debiasing, we adhere to the previous methods [16, 20] by utilizing a test set, which exclusively comprises bias-conflicting points from the unbiased test set. It is notable that the test set of BAR is composed solely of bias-conflicting samples, introducing a significant challenge for evaluation. Our primary metric is classification accuracy. We calculate aligned accuracy and conflicting accuracy separately for some of the ablations on CMNIST and C-CIFAR10 presented in Sec. 4.4. Aligned accuracy is computed solely on bias-aligned data points while conflicting accuracy is determined exclusively based on the bias-conflicting points. We conduct five independent trials with different random seeds and report both the mean and standard deviation to ensure statistical robustness.

Methods	Group	CMNIST				C-CIFAR10			
		Info	0.5	1.0	2.0	5.0	0.5	1.0	2.0
Group DRO	✓	63.12	68.78	76.30	84.20	33.44	38.30	45.81	57.32
ERM	✗	35.19 (3.49)	52.09 (2.88)	65.86 (3.59)	82.17 (0.74)	23.08 (1.25)	25.82 (0.33)	30.06 (0.71)	39.42 (0.64)
JTT	✗	53.03 (3.89)	62.9 (3.01)	74.23 (3.21)	84.03 (1.10)	24.73 (0.60)	26.90 (0.31)	33.40 (1.06)	42.20 (0.31)
LfF	✗	52.50 (2.43)	61.89 (4.97)	71.03 (2.44)	84.79 (1.09)	28.57 (1.30)	33.07 (0.77)	39.91 (0.30)	50.27 (1.56)
DFA	✗	65.22 (4.41)	81.73 (2.34)	84.79 (0.95)	89.66 (1.09)	29.95 (0.71)	36.49 (1.79)	41.78 (2.29)	51.13 (1.28)
LC	✗	71.25 (3.17)	82.25 (2.11)	86.21 (1.02)	91.16 (0.97)	34.56 (0.69)	37.34 (1.26)	47.81 (2.00)	54.55 (1.26)
DeNetDM	✗	74.72 (0.99)	85.22 (0.76)	89.29 (0.51)	93.54 (0.22)	38.93 (1.16)	44.20 (0.77)	47.35 (0.70)	56.30 (0.42)

Table 1: Performance in terms of accuracy is evaluated on test sets of CMNIST and C-CIFAR10, considering diverse percentages of bias-conflicting samples. Baseline method results are derived from [20] since we utilize identical experimental settings. Model requirements for spurious attribute annotations (type) are indicated by ✗ (not required) and ✓ (required). Best performances for each dataset are marked in **bold**.

Implementation details: We perform extensive hyperparameter tuning using a small unbiased validation set with bias annotations to obtain the deep and shallow branches for all the datasets. We consistently utilize the same debiasing model architectures used by the previous methods for our target branch to ensure a fair comparison. Additionally, a linear layer is employed for the classifier for all the datasets. The additional architecture details for different datasets are as follows:

- **CMNIST:** we use an MLP with three hidden layers for the deep branch and an MLP with a single hidden layer corresponding to the shallow branch. During the second phase of DeNetDM, we use an MLP with three hidden layers for the target branch.
- **C-CIFAR10, BAR:** we use the ResNet-20 architecture for the deep branch and a 3-layered CNN model for the shallow branch. The target branch used in the second stage of DeNetDM is ResNet-18.
- **BFFHQ:** we use the ResNet-18 architecture as the biased branch and a 4-layered CNN as the shallow branch. We also use the ResNet-18 architecture for the target branch, following the approaches of [16, 20].

Further details on the datasets and implementation are presented in Section D of the supplementary.

4.2 Evaluation Results

We present a comprehensive comparison of DeNetDM with all the baselines described in Sec. 4.1 across varying bias conflicting ratios on CMNIST, C-CIFAR10, BFFHQ and BAR in Tab. 1 and Tab. 2 respectively. As evident from Tab. 1 and Tab. 2, DeNetDM consistently outperforms all baselines across different bias ratios for CMNIST, BFFHQ and BAR datasets. Notably, on the C-CIFAR10 dataset, DeNetDM exhibits superior performance when bias ratios are at 0.5%, 1%, and 5%, and closely aligns with LC [20] in the case of 2%. These findings provide empirical evidence for the practical applicability of DeNetDM. It is worth mentioning that the proposed approach demonstrates a significant performance enhancement across all datasets when compared to Group DRO, which relies on predefined knowledge of bias. DeNetDM achieves this improvement without any form of supervision on the bias, highlighting the effectiveness

Methods	Group	BAR		BFFHQ
		1.0	5.0	1.0
ERM	\times	57.65 (2.36)	68.60 (2.25)	56.7 (2.7)
JTT	\times	58.17 (3.30)	68.53 (3.29)	65.3 (2.5)
LfF	\times	57.71 (3.12)	67.48 (0.46)	62.2 (1.6)
DFA	\times	52.31 (1.00)	63.50 (1.47)	63.9 (0.3)
LC	\times	70.94 (1.46)	74.32(2.42)	70.0 (1.4)
DeNetDM (ours)	\times	73.84 (2.56)	79.61 (3.18)	75.7 (2.8)

Table 2: Performance in terms of accuracy is evaluated on test sets of BAR and BFFHQ, considering diverse percentages of bias-conflicting samples. Additionally, both BAR and BFFHQ are evaluated on the test set which contains bias-conflicting samples. Baseline method results are derived from [18] for BAR and [20] for BFFHQ since we utilize identical experimental settings.

of depth modulation in the debiasing process. An intriguing observation from Tab. 1 is that DeNetDM demonstrates better performance compared to the baselines when the bias-conflicting ratio is lower, particularly evident in the C-CIFAR10 dataset. We believe that the effectiveness of inductive bias enforced by DeNetDM in distinguishing between core and bias attributes is superior to that of LC, thereby allowing it to adeptly capture core attributes even when dealing with data points that exhibit fewer bias conflicting points. This emphasizes the applicability of DeNetDM in scenarios where the training data exhibits a significant amount of spurious correlations. Another noteworthy observation in Tab. 2 is that DeNetDM outperforms LC and DFA by a considerable margin across all datasets, particularly on the complex real-world datasets, BAR and BFFHQ. Both LC and DFA rely on augmentations to enhance the diversity of bias-conflicting points, whereas our approach utilizes depth modulation to efficiently capture the core attribute characteristics in the existing training data. Despite this, DeNetDM still achieves superior performance compared to LC and DFA without relying on augmentations.

4.3 Analysis of Training Dynamics

In Sec. 3.1, we discussed the variability in the linear decodability at various depths and how the disparity in linear decodability between biased attributes and target attributes forms a significant motivation for debiasing. To further validate this intuition and identify the elements contributing to its effectiveness, we delve into the analysis of the training dynamics of DeNetDM during the initial training stages. We consider the training of Colored MNIST with 1% skewness due to its simplicity and ease of analysis. Figure 4 shows how linear decodability of attributes varies across different branches of DeNetDM during training. As depicted in Fig. 4, prior to the training, the deep branch demonstrates lower linear decodability for both the digit (core attribute) and color (bias attribute) in comparison to the linear decodability observed in the shallow branch. As the training process unfolds, the bias attribute which is relatively easier to learn, undergoes a rapid increase in the linear decodability in both the shallow and deep branches, as denoted by the label ‘A’ in Fig. 4. At this point, the disparity in linear decodability between the digit and color attributes becomes more pronounced in the deep branch as opposed to the shallow branch in the DeNetDM. This distinction serves as a prior, influencing the deep branch to effectively capture the bias.

Since we employ Product of Experts technique, the deep branch becomes proficient in classification using the spurious attribute, thereby compelling the shallow branch to rely on other attributes such as digit for the classification. It is worth noting that the linear decodability of core attributes is more pronounced in the shallow branch, allowing them to capture the core attributes. Therefore, the training paradigm of DeNetDM leads to a shallow branch that is robust to spurious correlations, and a deep branch that predominantly relies on the biased attribute. This analysis not only confirms our intuition but also furnishes empirical evidence that the training paradigm is effective in the process of debiasing.

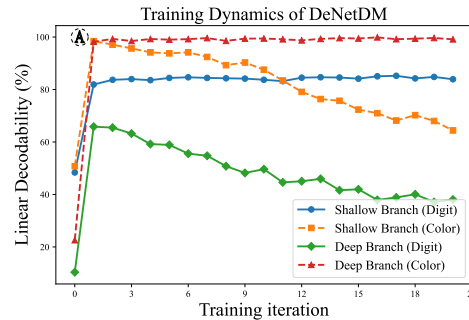


Fig. 4: Training dynamics of DeNetDM during initial stages of training monitored in terms of linear decodability of bias attribute (color) and core attribute (digit).

4.4 Ablation Studies

We perform several ablation studies to evaluate different facets of DeNetDM. Initially, we explore the influence of network depth, a fundamental element of DeNetDM. Additionally, we scrutinize the effect of various loss components on the performance of DeNetDM. Lastly, we conduct an analysis to ascertain the sensitivity of our approach to the number of parameters. All the experiments in this section are conducted on CMNIST and C-CIFAR10 datasets where the ratio of conflicting points is set to 1%.

Effect of depth modulation: To validate our hypothesis regarding the significance of network depth in DeNetDM, we conduct an ablation by setting the same depth for both the branches which is then compared with the default DeNetDM where one branch is deeper compared to the other. We perform the first stage of DeNetDM training for 5 different random seeds and the averaged test accuracy on bias-aligned points and bias-conflicting for individual branches are reported in Tab. 3. Branch 1 and Branch 2 in Tab. 3 correspond to the deep and shallow branches in DeNetDM respectively. We ignore the second stage of training in this case since we majorly focus on the segregation of bias and core attributes. One interesting observation is that DeNetDM exhibits a huge standard deviation in the accuracies when the branches are of the same depth which is evident in both datasets. This phenomenon arises because DeNetDM, in such a configuration, loses its ability to clearly distinguish between the branches since the feature decodability of bias and core attributes would be almost similar in both the branches as discussed in Sec. 3.1. As a result, DeNetDM either distributes information across multiple branches or, alternatively, it may still separate core and bias attributes, but the specific branch capturing core attributes varies with different initialization. In contrast, when the depths are unequal for

both datasets, the deeper branch tends to disregard conflicting points and concentrate on the aligned points, as evident from the test accuracies provided in Tab. 3. Additionally, the shallow branch emphasizes capturing core attributes and thus consistently enhancing the conflicting accuracy. This shows the pivotal role of depth modulation in the DeNetDM framework for effectively segregating bias and core attributes.

We also examine the early training dynamics of ResNet-8, ResNet-32, and ResNet-50, akin to Fig. 2b in C-CIFAR10 dataset to assess the scalability of DeNetDM to larger ResNet models. After 200 iterations, texture (bias)

decodability in all architectures neared 99%, while core attribute decodability for ResNet-8, ResNet-32, and ResNet-50 was 18.74%, 24.32%, and 12.91%, respectively. This aligns with our hypothesis that ResNet-50 would prefer texture attribute over core when paired with ResNet-8 or ResNet-32. To confirm, we tested two setups: (1) ResNet-8 and ResNet-50, and (2) ResNet-32 and ResNet-50. The results, shown in Tab. 3, indicate high bias-aligned accuracy for ResNet-50 and high bias-conflicting accuracy for ResNet-8 and ResNet-32 respectively. Since ResNet-50 has lower core attribute decodability than ResNet-8 and ResNet-32, it favors bias attributes, while the shallow branches capture core attributes. This experimental results suggest DeNetDM’s applicability to diverse, complex and larger models / architectures.

Effect of loss components: To assess the impact of various loss components, we conduct ablation studies by selectively removing components and analyzing their effects on classification accuracy, specifically on the test set, as well as accuracy on bias-aligned and bias-conflicting points. The results of the study are presented in Tab. 4. As observed from Tab. 4, when considering \mathcal{L}_{CE} alone which corresponds to the first stage of DeNetDM involving depth modulation, the model exhibits a relatively strong ability to learn the target attributes, achieving 37.42% and 83.28% accuracy on C-CIFAR10 and CMNIST, respectively. However, upon introducing the second stage of DeNetDM training with \mathcal{L}_t alone, the target model tends to capture a significant amount of bias information alongside core attributes compared to the robust model obtained in the first stage. This is evident from the high accuracy on aligned points, reaching 81.60% and 95.85% on C-CIFAR10 and CMNIST, respectively. When introducing \mathcal{L}_{dist} alone, the model distills knowledge from the

Dataset	Depth (Branch 1, Branch 2)	Branch	Conflicting Accuracy (%)	Aligned Accuracy (%)
CMNIST	(5, 5)	Branch 1	44.94 (22.25)	74.85 (12.71)
		Branch 2	17.25 (7.89)	88.57 (9.50)
	(5, 3)	Branch 1	1.921 (0.29)	99.92 (0.25)
		Branch 2	83.17 (0.96)	88.25 (2.254)
C-CIFAR10	(ResNet-20, ResNet-20)	Branch 1	19.54 (11.16)	85.83 (8.19)
		Branch 2	24.42 (16.93)	86.95 (11.04)
	(ResNet-20, 3-layer CNN)	Branch 1	3.0 (1.29)	99.34 (0.47)
		Branch 2	38.52 (0.99)	76.72 (2.19)
(ResNet-50, ResNet-32)	Branch 1	3.48 (0.98)	97.15 (2.10)	
	Branch 2	30.88 (1.22)	81.72 (0.73)	
(ResNet-50, ResNet-8)	Branch 1	9.38 (1.52)	98.60 (0.86)	
	Branch 2	20.32 (1.90)	59.94 (2.61)	

Table 3: Comparison of the performance of DeNetDM using different network depths for the two branches of DeNetDM.

Idx	Dataset	\mathcal{L}_{CE} (Stage-1)	\mathcal{L}_{dist} (Stage-2)	\mathcal{L}_t (Stage-2)	Accuracy (%)	Conflicting Accuracy (%)	Aligned Accuracy (%)
1	C-CIFAR10	✓	-	-	37.47	37.42	72.40
2	C-CIFAR10	✓	-	✓	42.89	35.74	81.60
3	C-CIFAR10	✓	✓	-	42.25	38.34	68.52
4	C-CIFAR10	✓	✓	✓	43.12	39.46	69.53
1	CMNIST	✓	-	-	81.61	83.28	89.66
2	CMNIST	✓	-	✓	82.96	81.53	95.85
3	CMNIST	✓	✓	-	84.05	83.41	89.86
4	CMNIST	✓	✓	✓	84.97	84.44	89.17

Table 4: Ablation study of different losses used in DeNetDM.

shallow branch obtained in the first stage, resulting in the target model exhibiting a similar performance as that of the stage 1 training. However, performing the second stage of DeNetDM training using both \mathcal{L}_t and $\mathcal{L}_{\text{dist}}$ prevents the model from capturing bias, thus focussing more on learning the core features. This leads to improved conflicting and overall accuracy.

Sensitivity to number of parameters: We also investigate the influence of the number of parameters of both branches on DeNetDM performance. We opt for the optimal configuration of the proposed approach on C-CIFAR10 and conducted an ablation study, employing ResNet-20 ($\text{depth}(\phi_b) = 20$) as the deep network and a 3-layer CNN ($\text{depth}(\phi_d) = 3$) as the shallow network. We explore three scenarios where $|\phi_b| < |\phi_d|$, $|\phi_b| \approx |\phi_d|$, and $|\phi_b| > |\phi_d|$. The first stage of DeNetDM training is then performed to analyze learning in the deep and shallow models in each of the cases, and the results are presented in Tab. 5.

As indicated in Tab. 5, the shallow model exhibits increased resilience to spurious correlations, while the deep model captures bias in all three cases. This suggests that DeNetDM effectively segregates bias and core attributes regardless of the number of parameters in both branches. Interestingly, a notable finding is

that the shallow model exhibits better robustness against correlations when the shallow branch possesses a greater number of parameters compared to the deep model, as evident from Tab. 5. We also perform a similar ablation on the CMNIST dataset and the results are provided in Section C of the supplementary.

Case	Branch	Conflicting Accuracy (%)	Aligned Accuracy (%)
$\phi_b > \phi_d$	ϕ_b	3.08	96.8
	ϕ_d	29.78	62.61
$\phi_b \approx \phi_d$	ϕ_b	3.48	95.91
	ϕ_d	28.64	64.32
$\phi_b < \phi_d$	ϕ_b	2.04	99.01
	ϕ_d	39.05	67.68

Table 5: Ablation study on the number of parameters of deep and shallow branches in DeNetDM using C-CIFAR10 dataset.

5 Conclusion

We introduce a novel debiasing method that leverages the variations in linear decodability across network depths. Through an extensive analysis of bias and core attributes across networks of varying depths, we uncover compelling insights into the interplay between network architecture, attribute decodability, and training methodologies. Leveraging these insights, we present a training approach derived from the Product of Experts methodology by employing paired deep and shallow branches and then transferring their debiasing capabilities to the desired architecture. By modulating the network depths, DeNetDM adeptly captures core attributes within the debiased model without necessitating explicit reweighting or data augmentation. We conducted extensive experiments and meticulous ablation studies across various datasets, including synthetic datasets like Colored MNIST and Corrupted CIFAR-10, along with real-world datasets, Biased FFHQ and BAR, to validate the robustness and superiority of our methodology. Significantly, we present empirical evidence demonstrating that DeNetDM achieves comparable performance to supervised approaches, despite not having access to bias annotations.

References

1. Ahuja, K., Shanmugam, K., Varshney, K., Dhurandhar, A.: Invariant risk minimization games. In: ICML (2020) [9](#)
2. Allen-Zhu, Z., Li, Y.: Towards understanding ensemble, knowledge distillation and self-distillation in deep learning. In: ICLR (2023) [4](#)
3. Asif, U., Tang, J., Harrer, S.: Ensemble knowledge distillation for learning improved and efficient networks. In: ECAI (2020) [4](#)
4. Choi, S., Kim, J.T., Choo, J.: Cars can't fly up in the sky: Improving urban-scene segmentation via height-driven attention networks. In: Proceedings of the IEEE/CVF Conference on Computer Vision and Pattern Recognition (CVPR) (June 2020) [1](#)
5. Clark, C., Yatskar, M., Zettlemoyer, L.: Don't take the easy way out: Ensemble based methods for avoiding known dataset biases. In: EMNLP-IJCNLP (2019) [3](#)
6. Diffenderfer, J., Bartoldson, B.R., Chaganti, S., Zhang, J., Kailkhura, B.: A winning hand: Compressing deep networks can improve out-of-distribution robustness. In: NeurIPS (2021) [4](#)
7. Ge, S., Mishra, S., Li, C.L., Wang, H., Jacobs, D.: Robust contrastive learning using negative samples with diminished semantics. In: NeurIPS (2021) [3](#)
8. Geirhos, R., Rubisch, P., Michaelis, C., Bethge, M., Wichmann, F.A., Brendel, W.: Imagenet-trained CNNs are biased towards texture; increasing shape bias improves accuracy and robustness. In: ICLR (2019) [2, 3](#)
9. Hendrycks, D., Dietterich, T.: Benchmarking neural network robustness to common corruptions and perturbations. In: ICLR (2019) [9](#)
10. Hermann, K., Lampinen, A.: What shapes feature representations? exploring datasets, architectures, and training. In: NeurIPS (2020) [2, 3, 5](#)
11. Hinton, G.E.: Training products of experts by minimizing contrastive divergence. *Neural Comput.* (2002) [2, 3, 4, 7](#)
12. Karimi Mahabadi, R., Belinkov, Y., Henderson, J.: End-to-end bias mitigation by modelling biases in corpora. In: ACL (2020) [3](#)
13. Karras, T., Laine, S., Aila, T.: A style-based generator architecture for generative adversarial networks. In: CVPR (2019) [9](#)
14. Kim, B., Kim, H., Kim, K., Kim, S., Kim, J.: Learning not to learn: Training deep neural networks with biased data. In: CVPR (2019) [2, 3](#)
15. Kim, E., Lee, J., Choo, J.: Biaswap: Removing dataset bias with bias-tailored swapping augmentation. In: ICCV (2021) [1, 2, 4, 9](#)
16. Lee, J., Kim, E., Lee, J., Lee, J., Choo, J.: Learning debiased representation via disentangled feature augmentation. In: NeurIPS (2021) [2, 4, 8, 9, 10](#)
17. Lee, J., Park, J., Kim, D., Lee, J., Choi, E., Choo, J.: Revisiting the importance of amplifying bias for debiasing. In: AAAI (2023) [4](#)
18. Lim, J., Kim, Y., Kim, B., Ahn, C., Shin, J., Yang, E., Han, S.: Biasadv: Bias-adversarial augmentation for model debiasing. In: Proceedings of the IEEE/CVF Conference on Computer Vision and Pattern Recognition (CVPR) (2023) [11](#)
19. Liu, E.Z., Haghgoo, B., Chen, A.S., Raghunathan, A., Koh, P.W., Sagawa, S., Liang, P., Finn, C.: Just train twice: Improving group robustness without training group information. In: ICML (2021) [8, 9](#)
20. Liu, S., Zhang, X., Sekhar, N., Wu, Y., Singhal, P., Fernandez-Granda, C.: Avoiding spurious correlations via logit correction. In: ICLR (2023) [4, 9, 10, 11](#)
21. Majumdar, P., Singh, R., Vatsa, M.: Attention aware debiasing for unbiased model prediction. In: ICCVW (2021) [2, 3](#)
22. Mehrabi, N., Morstatter, F., Saxena, N., Lerman, K., Galstyan, A.: A survey on bias and fairness in machine learning. *ACM Comput. Surv.* (2021) [3](#)

23. Nam, J., Cha, H., Ahn, S., Lee, J., Shin, J.: Learning from failure: De-biasing classifier from biased classifier. In: NeurIPS (2020) [2](#), [4](#), [5](#), [8](#), [9](#)
24. Park, G.Y., Lee, S., Lee, S.W., Ye, J.C.: Training debiased subnetworks with contrastive weight pruning. In: CVPR (2023) [4](#)
25. Qi, J., Tang, K., Sun, Q., Hua, X.S., Zhang, H.: Class is invariant to context and vice versa: On learning invariance for out-of-distribution generalization. In: Computer Vision – ECCV 2022: 17th European Conference, Tel Aviv, Israel, October 23–27, 2022, Proceedings, Part XXV (2022) [9](#)
26. Sagawa, S., Koh, P.W., Hashimoto, T.B., Liang, P.: Distributionally robust neural networks for group shifts: On the importance of regularization for worst-case generalization. In: ICLR (2020) [2](#), [3](#), [9](#)
27. Seo, S., Lee, J.Y., Han, B.: Unsupervised learning of debiased representations with pseudo-attributes. In: CVPR (2022) [4](#)
28. Shah, H., Tamuly, K., Raghunathan, A., Jain, P., Netrapalli, P.: The pitfalls of simplicity bias in neural networks. In: Larochelle, H., Ranzato, M., Hadsell, R., Balcan, M., Lin, H. (eds.) NeurIPS (2020) [1](#)
29. Shrestha, R., Kafle, K., Kanan, C.: Occamnets: Mitigating dataset bias by favoring simpler hypotheses. In: ECCV (2022) [4](#)
30. Sohoni, N., Dunnmon, J., Angus, G., Gu, A., Ré, C.: No subclass left behind: Fine-grained robustness in coarse-grained classification problems. In: NeurIPS (2020) [4](#)
31. Tiwari, R., Shenoy, P.: Overcoming simplicity bias in deep networks using a feature sieve. In: ICML (2023) [4](#)
32. Vapnik, V.: An overview of statistical learning theory. IEEE TNN (1999) [9](#)
33. Wang, H., He, Z., Lipton, Z.L., Xing, E.P.: Learning robust representations by projecting superficial statistics out. In: ICLR (2019) [3](#)
34. Wang, Z., Qinami, K., Karakozis, I., Genova, K., Nair, P., Hata, K., Russakovsky, O.: Towards fairness in visual recognition: Effective strategies for bias mitigation. In: CVPR (2020) [2](#), [3](#)
35. Zhang, D., Ahuja, K., Xu, Y., Wang, Y., Courville, A.: Can subnetwork structure be the key to out-of-distribution generalization? In: ICML (2021) [4](#)
36. Zhang, H., Cissé, M., Dauphin, Y.N., Lopez-Paz, D.: mixup: Beyond empirical risk minimization. In: ICLR (2018) [9](#)

DeNetDM : Supplementary material

No Author Given

No Institute Given

Table of Contents

DeNetDM : Supplementary material	1
<i>No Author Given</i>	

A Introduction

In the primary text of our submission, we introduce DeNetDM, a novel debiasing framework that leverages the variation of linear decodability across network depths to effectively disentangle bias from core attributes. This technique sets a new benchmark for bias mitigation, achieving unparalleled performance without reliance on data augmentations. To ensure our manuscript's integrity, we provide extensive supplementary material designed to complement the main text. This includes a series of additional experiments, expanded ablation studies, comprehensive implementation protocols, and deeper analyses of our findings. The supplementary sections are presented to bridge the content gap necessitated by the page constraints of the main manuscript, providing a detailed exposition of our methodology and its broader impact on the domain.

B Equivalence with Product of Experts Framework

In section 3.2 of the main text, we asserted that our training methodology is derived from the Product of Experts. In this section, we elucidate this mathematically:

$$f : \mathbb{R}^F \xrightarrow{\text{linear}} \mathbb{R}^c, \quad \tilde{f}(x) = \text{softmax}(f(x))$$

$$\phi_b : \mathbb{R}^{C \times H \times W} \longrightarrow \mathbb{R}^F, \quad \text{where } F \text{ is the feature dimension}$$

$$\phi_d : \mathbb{R}^{C \times H \times W} \longrightarrow \mathbb{R}^F, \quad \text{such that } \text{depth}(\phi_b) > \text{depth}(\phi_d)$$

$$\begin{aligned}
L(x, y; \phi_b, \phi_d) &= - \sum_{c=1}^C y_c \log(\hat{p}_{\phi_b, \phi_d}^c) \quad (\text{Loss function definition}) \\
\hat{p}_{\phi_b, \phi_d} &= \frac{\tilde{f}_c(\phi_b(x)) \cdot \tilde{f}_c(\phi_d(x))}{\sum_{c=1}^C \tilde{f}_c(\phi_b(x)) \cdot \tilde{f}_c(\phi_d(x))} \quad (\text{Product of Experts}) \\
&= \text{softmax}_c(\log(\tilde{f}(\phi_b(x))) + \log(\tilde{f}(\phi_d(x)))) \quad (\text{Softmax log-sum-exp trick}) \\
&= \text{softmax}_c(f(\phi_b(x)) + f(\phi_d(x))) \quad (\text{Translation invariance of softmax}) \\
&= \text{softmax}_c(f(\phi_b(x) + \phi_d(x))) \quad (\text{Linearity of classifier } f)
\end{aligned}$$

We utilize \hat{p}_{ϕ_b, ϕ_d} to compute the probabilities in DeNetDM which is the same as Equation 2 presented in the main paper.

C Additional Experiments

C.1 Depth vs. Number of parameters

DeNetDM employs depth modulation as its principal strategy for mitigating bias. The primary text, constrained by spatial limitations, only includes an ablation study detailing the influence of depth modulation on the C-CIFAR10 dataset. However, this section extends the scope of our analysis to encompass the CMNIST dataset. The findings for CMNIST mirror those observed for C-CIFAR10: the shallow branch demonstrates robustness to spurious correlations, whereas the deep branch consistently assimilates bias irrespective of the number of parameters in both branches. These consistent patterns across datasets reinforce the efficacy of DeNetDM in distinguishing between bias and core attributes.

Case	Branch	Conflicting Accuracy (%)	Aligned Accuracy (%)
$\phi_b < \phi_d$	ϕ_b	11.90	99.93
	ϕ_d	83.89	88.78
$\phi_b \approx \phi_d$	ϕ_b	11.87	99.90
	ϕ_d	83.07	89.09
$\phi_b > \phi_d$	ϕ_b	10.79	98.26
	ϕ_d	83.32	88.61

Table 1: Ablation study on the number of parameters of deep and shallow branches in DeNetDM using CMNIST dataset.

C.2 Effect of Network Depth on DeNetDM

In the main text, we have illustrated how the variation in network depth affects the performance of DeNetDM. We provide an in-depth analysis in this section. As observed in the first three rows of Tab. 2, as the difference in network depth of deep and shallow progressively increases, the performance of the debiased model

increases monotonically. Further, when we decrease the difference in depth of shallow and deep branches (rows 3 and 4) the performance decreases to 80.42% compared to 87.37%. Similar performance degradation can be seen when we increase the depth of the shallow network from 4 to 6 (rows 5 and 6). Hence, DeNetDM is able to distinguish bias and core attributes better when there is a significant difference between the depths of shallow and deep branches. This aligns with the observations presented in Section 4.4 of the main text (Effect of depth modulation).

Depth (Shallow, Deep)	Conflicting Accuracy (%)	Aligned Accuracy(%)
(3, 4)	72.20	98.33
(3, 5)	80.46	92.87
(3, 7)	87.37	93.62
(6, 7)	80.42	96.45
(4, 8)	91.19	94.62
(6, 8)	69.55	93.83

Table 2: Performance comparison of DeNetDM for various depths of shallow and deep branches.

C.3 Performance on varying bias-conflicting ratios

We perform experiments on the CMNIST dataset with bias-conflicting ratios of 10% and 20% to evaluate our method’s efficacy across a broader range of ratios. The findings, presented in Tab. 3, show that DeNetDM performs as expected, effectively capturing core attributes in the shallow branch for varied bias ratios.

Bias ratio	Branch	Conflicting Accuracy (%)	Aligned Accuracy (%)
10%	Deep	1.84(0.5)	99.14(0.2)
	Shallow	93.12(0.8)	96.47(1.3)
20%	Deep	3.23(2.8)	97.93(2.1)
	Shallow	94.49(2.4)	97.51(3.4)

Table 3: Results on CMNIST with wider bias conflicting ratios.

D Additional details

In this section, we provide an in-depth discussion of various datasets used along with finer implementation details that enhance the reproducibility of our method.

D.1 Datasets

We provide a detailed description of various datasets used along with a representative sample of all of them.

- **Colored MNIST(CMNIST):** CMNIST is an adaptation of the MNIST, that introduces color variation to the images. For each digit class, the majority $(1 - \alpha)$ of the images are correlated with the corresponding color c_i , with

i matching the digit label y . The remaining images are randomly assigned one of the other colors c_j , where $j \neq y$. The challenge of this dataset lies in identifying the digits despite the strong color bias. To incorporate color variability, a noise vector v drawn from a normal distribution is added to c_i . The dataset and its characteristics are illustrated in Fig. 1. Among multiple choices of severity, we choose the most severe corruption to simulate the worst-case scenario as done in other works.

- **Corrupted CIFAR10 (C-CIFAR10)**: The Corrupted CIFAR dataset represents an evolved form of the classic CIFAR set, with an emphasis on two particular features: the object depicted and the type of corruption applied. In an approach akin to that used for CMNIST, this dataset adopts an array of corruption styles, labeled from c_0 , symbolizing blurring, to c_9 , indicative of snow. Within each object category, a proportion $1 - \alpha$ of the images is intentionally altered with the corruption type c_i , corresponding to the object’s label y . The remainder of the images is processed with a randomly selected corruption type c_j , chosen to ensure $j \neq y$. In our dataset, we employ the highest degree of corruption out of the five levels outlined in the original CMNIST dataset. Illustrative samples from this dataset are demonstrated in Fig. 1.
- **Biased FFHQ (BFFHQ)**¹ The BFFHQ dataset is a selectively reduced subset derived from the larger FFHQ database of facial images, with a focus on the attributes of gender and age. Gender is designated as the primary attribute of analysis, with age being the secondary attribute that could introduce bias. The gender classification is binary, encompassing male and female categories. The dataset predominantly features male images of subjects aged between 40 and 59, whereas female images are generally of subjects aged between 10 and 29. Samples that defy these age associations—such as younger male or older female subjects—are also present, offering a counterpoint to the main age distribution.

D.2 Implementation details

In this section, we detail the optimal hyperparameters identified for various datasets, which were instrumental in achieving the results reported in the main manuscript. The optimal hyperparameters obtained for various datasets are listed in Tab. 4. Additional parameters not mentioned in Tab. 4 follow the default values of Pytorch.

Data Augmentations: The training phase of DeNetDM incorporated specific data augmentation techniques tailored to each dataset. For instance, the CMNIST dataset did not utilize any form of augmentation. In contrast, the C-CIFAR10 and BFFHQ datasets applied Random Horizontal Flip and random cropping, with the latter involving crops from images padded by 4 pixels. These augmentations are critical as they introduce variability into the dataset, aiding the generalization ability of the neural network.

¹ <https://github.com/kakaoenterprise/Learning-Debiased-Disentangled>



Fig. 1: Samples from training data of CMNIST, Corrupted-CIFAR10 and Biased FFHQ.

Architectural Details: Depth modulation is a critical component of our de-biasing strategy. Below we enumerate the architecture specifics of the shallow branches tailored for each dataset.

CMNIST:

```
(shallow branch): Sequential(
  (c1): Linear(in_features=2352, out_features=100, bias=True)
  (r1): ReLU()
  (s1): MLPHiddenlayers(
    (hidden_layers): ModuleList(
      (0): Linear(in_features=100, out_features=100, bias=True)
    )
    (act): ReLU()
  )
)
```

C-CIFAR10 and BAR:

```
(shallow branch): Sequential(
  (c1): Conv2d(3, 32, kernel_size=(5, 5), stride=(1, 1))
  (b1): BatchNorm2d(32, eps=1e-05, momentum=0.1, affine=True,
    track_running_stats=True)
  (r1): ReLU()
  (s1): MaxPool2d(kernel_size=(2, 2), stride=2, padding=0, dilation=1,
    ceil_mode=False)
  (c2): Conv2d(32, 64, kernel_size=(5, 5), stride=(1, 1))
  (b2): BatchNorm2d(64, eps=1e-05, momentum=0.1, affine=True,
    track_running_stats=True)
  (r2): ReLU()
  (s2): MaxPool2d(kernel_size=(2, 2), stride=2, padding=0, dilation=1,
    ceil_mode=False)
  (c3): Conv2d(64, 64, kernel_size=(5, 5), stride=(1, 1))
  (b3): BatchNorm2d(64, eps=1e-05, momentum=0.1, affine=True,
    track_running_stats=True)
  (r3): ReLU()
)
```

```
(f1): Flatten(start_dim=1, end_dim=-1)
)
(classifier): Linear(in_features=64, out_features=10, bias=True)
(act): ReLU()
```

BFFHQ:

```
(shallow branch): Sequential(
  (c1): Conv2d(3, 64, kernel_size=(7, 7), stride=(1, 1))
  (b1): BatchNorm2d(64, eps=1e-05, momentum=0.1, affine=True,
    track_running_stats=True)
  (r1): ReLU(inplace=True)
  (s1): MaxPool2d(kernel_size=(2, 2), stride=2, padding=0, dilation=1,
    ceil_mode=False)
  (c2): Conv2d(64, 128, kernel_size=(3, 3), stride=(1, 1))
  (b2): BatchNorm2d(128, eps=1e-05, momentum=0.1, affine=True,
    track_running_stats=True)
  (r2): ReLU(inplace=True)
  (s2): MaxPool2d(kernel_size=(2, 2), stride=2, padding=0, dilation=1,
    ceil_mode=False)
  (c3): Conv2d(128, 512, kernel_size=(3, 3), stride=(1, 1))
  (s3): MaxPool2d(kernel_size=(2, 2), stride=2, padding=0, dilation=1,
    ceil_mode=False)
  (b3): BatchNorm2d(512, eps=1e-05, momentum=0.1, affine=True,
    track_running_stats=True)
  (r3): ReLU(inplace=True)
  (c4): Conv2d(512, 512, kernel_size=(3, 3), stride=(1, 1))
  (b4): BatchNorm2d(512, eps=1e-05, momentum=0.1, affine=True,
    track_running_stats=True)
  (r4): ReLU(inplace=True)
  (a1): AdaptiveAvgPool2d(output_size=(1, 1))
  (f1): Flatten(start_dim=1, end_dim=-1)
)
```

Parameter	CMNIST	C-CIFAR10, BAR	BFFHQ
Learning Rate (LR)	$(1.0 \times 10^{-3}, 1.0 \times 10^{-3})$	$(1.0 \times 10^{-3}, 1.0 \times 10^{-4})$	$(1.0 \times 10^{-3}, 1.0 \times 10^{-4})$
Batch Size	(64, 64)	(256, 256)	(64, 64)
Momentum	0.900	0.900	0.900
Weight Decay	$(1.0 \times 10^{-3}, 0)$	$(1.0 \times 10^{-3}, 0)$	(0, 0)
Epochs	(100, 100)	(100, 200)	(10, 100)

Table 4: Optimal hyperparameters for the CMNIST, C-CIFAR10, and BFFHQ datasets determined through extensive experimentation. The tuples represent optimal hyperparameters for Stage 1 and Stage 2, respectively.

E Limitations & Broader Impact

The primary challenge with this approach is the scalability issue when applied to a multi-bias setting. As the number of bias attributes increases, the subtle variations in linear decodability across the various branches could become so refined that accurately identifying biases may fail to achieve high fidelity. Moreover, depending on the network architecture might compel the model to depend excessively on intricate hyperparameter adjustments.